# Size Scaling and Nondiffusive Features of Electron Heat Transport in Multi-Scale Turbulence

Z. Lin[1], Y. Xiao[1], W. J. Deng[1], I. Holod[1], C. Kamath[2], S. Klasky[3], Z. X. Wang[1], and H. S. Zhang[4,1]

[1]University of California, Irvine, CA 92697, USA
[2]Lawrence Livermore National Laboratory, Livermore, CA 94550, USA
[3]Oak Ridge National Laboratory, Oak Ridge, TN 37831, USA
[4]Fusion Simulation Center, Peking University, Beijing 100871, P.R. China

We report recent results from global gyrokinetic particle simulations of the collisionless trapped electron mode (CTEM) turbulence, turbulent momentum transport, and turbulent transport in the reverse shear toroidal plasmas. The study of CTEM turbulence shows that the presence of mesoscale structures drives a nondiffusive component in the electron heat flux due to the weak nonlinear detuning of the precessional resonance that excites the linear instability. The simulation of turbulent momentum transport finds conductive, pinch, and residual momentum fluxes. The study of turbulent transport in the reverse shear toroidal plasmas shows that, due to the turbulence spreading, the electrostatic drift wave turbulence itself does not support either linear or nonlinear mechanism for the formation of internal transport barriers in the reversed magnetic shear when $q_{\min}$ crossing an integer.

## 1. Introduction

The global gyrokinetic toroidal code (GTC) [1] simulations of the collisionless trapped electron mode (CTEM) turbulence [2] find that the electron heat transport exhibits a gradual transition from Bohm to gyro-Bohm scaling when device size is increased. Comprehensive analysis of radial correlation function indicates that the turbulence eddies are predominantly microscopic but with a significant component in the mesoscale. A comprehensive analysis of kinetic and fluid time scales finds very weak nonlinear detuning of the toroidal precessional resonance of the magnetically trapped electrons that drives the linear CTEM instability. Thus the trapped electrons behave as fluid elements in the transport process, and their ballistic radial drifts across the mesoscale eddies drive a nondiffusive component in the electron heat ux. The nondiffusive electron heat flux, together with the turbulence spreading, leads to an effective electron heat conductivity dependent on the device size.

In contrast, ion heat transport in the CTEM turbulence is diffusive due to a stochastic parallel wave-particle decorrelation. The parallel wave-particle decorrelation is not operational for trapped electrons because of the bounce-averaging by the fast parallel motion. The non-diffusive feature of the electron heat transport is further conformed by the probability distribution function (PDF) of the flux-surface-averaged heat fluxes. The electron heat flux has a significant component above the lognormal distribution indicating a superdiffusive process. The ballistic electron heat flux may be responsible for the experimental observations of the residual electron transport inside the internal transport barrier (ITB) where the ion transport is neoclassical.

CTEM turbulence spreading [3] is even more pronounced in a reversed shear tokamak. GTC simulation shows that the linear eigenmodes only appear in the normal shear region. After the saturation, the turbulence spreads across the $q_{min}$ surface into the reversed shear region with a front propagation speed of about half of the electron diamagnetic flow. The turbulence occupies the whole volume without any identifiable gap or coherent structures in the $q_{min}$ location or the reversed shear region. Our finding indicates that the electrostatic turbulence itself does not support linear or nonlinear mechanism for the formation of ITB in the reversed magnetic shear when $q_{min}$ crossing an integer.

Momentum transport is one of the topics of current interest in fusion research. The radial flux of toroidal angular momentum can generally be decomposed into a diagonal (conductive) and off-diagonal (convective and residual stress) parts. To gain a better understanding of the physics picture for the off-diagonal momentum transport, we run global gyrokinetic particle simulations with zero and finite background rotation in the presence of drift wave turbulence with kinetic electrons [4]. We find that the magnitude of the momentum flux scales with the system size according to the gyroBohm scaling, with no significant size effect on the radial structure of the perturbed toroidal angular momentum. The symmetry breaking due to the shear of the radial electric field is found to be a mechanism for generating the residual momentum flux. However, it is small compared with the momentum pinch term in the case of a finite background rotation. The trapped electrons in the ITG turbulence increase the intensity and modify the spectral properties of the electrostatic fluctuations, leading to the increase in the toroidal momentum pinch.

2. CTEM transport scaling and transport mechanism

We carried out a gyrokinetic particle simulation to study the drift turbulence based on the following parameters [2]: $R/L_{Te}=6.9$, $R/L_{Ti}=2.2$ for CTEM turbulence study ( $R/L_{Ti}=2.2$ for ITG turbulence study), $R/L_n=2.2$, $a/\rho_i=250$, $a/R_0=0.358$, $T_i/T_e=1.0$, $m_i/m_e=1837$, the safety factor $q=0.58+1.09r/a+1.09(r/a)^2$ , with $q=1.4$ and magnetic shear $s=0.78$ at $r=0.5a$ . A circular cross section model is used for the equilibrium magnetic field, $B=B_0/(1+r\cos\theta/R_0)$ with the simulation carried out in the annulus between $r=0.1a$ and $r=0.9a$ .

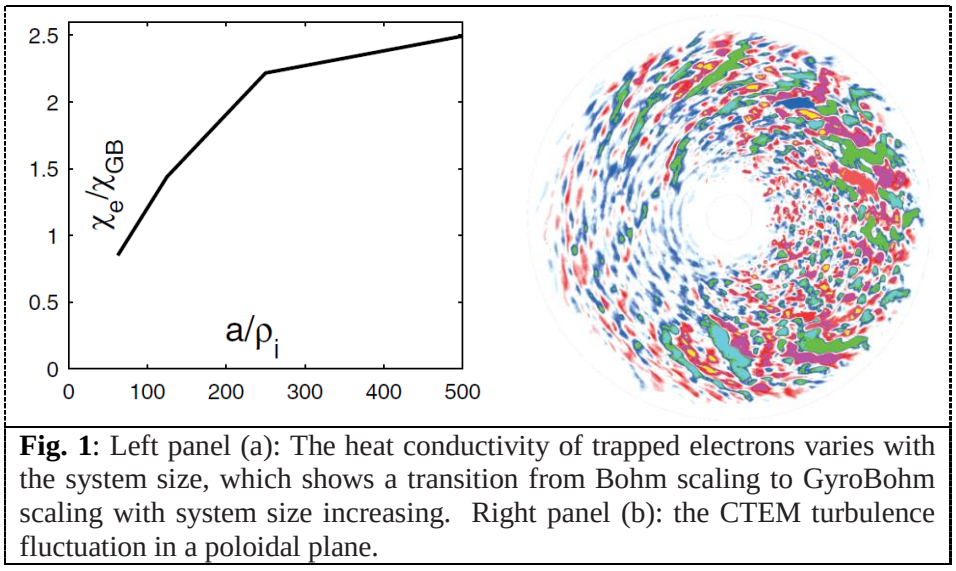


**Fig. 1**: Left panel (a): The heat conductivity of trapped electrons varies with the system size, which shows a transition from Bohm scaling to GyroBohm scaling with system size increasing. Right panel (b): the CTEM turbulence fluctuation in a poloidal plane.

First we examine the electron transport scaling with the system size in the CTEM turbulence. Figure 1(a) shows that the volume-averaged trapped electron heat conductivity $\chi_e$ varies with the system size $a/\rho_i$ , where $\chi_e$ is defined by $q_e=n_{tr}\chi_e\nabla T_e$, with $n_{tr}$ the trapped-electron density. When the system size is small, $a/\rho_i<250$, the electron heat transport clearly shows the Bohm scaling. When the system size increases, the electron heat transport gradually changes to the gyro-Bohm (GB) scaling with $\chi_e=2.5\chi_{GB}$, similar to the ion heat transport in the ITG turbulence [5]. Figure 1(b) shows the poloidal plane snapshots of the electrostatic potential after the nonlinear saturation. Zonal flows are self-consistently treated in the simulation. Despite the zonal flow shearing effects, a significant number of mesoscale eddies survive and induces a nondiffusive component on the mesoscale for the electron heat transport. Detailed 2D correlation analysis shows that the turbulence eddies for different

machine sizes have the same microscopic scale length with a significant component in the mesoscale which drives the electron transport away from the gyro-Bohm scaling [2].

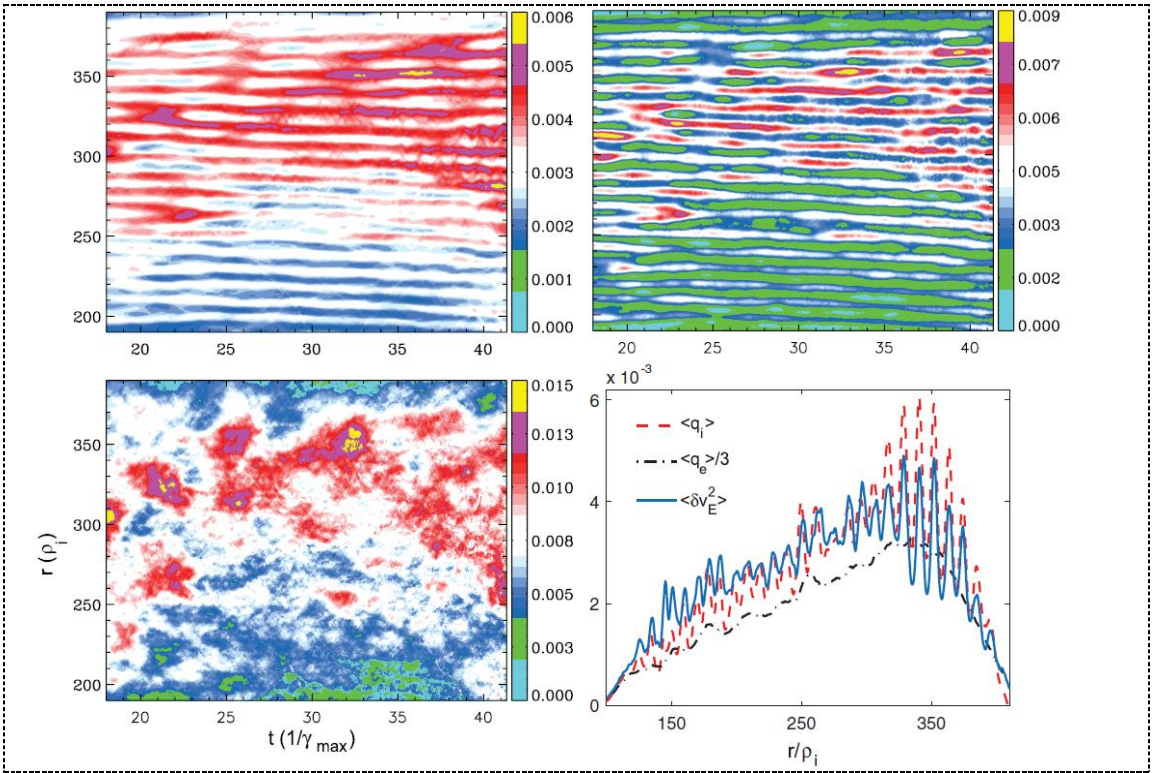


**Fig. 2**: CTEM turbulence: the time-radial contour plot is shown for ion heat flux $< q_i >$ in the top left panel (a), turbulence intensity $< \delta\phi^2 >$ in the top right panel (b), and electron heat flux $< q_e >$ in the lower left panel (c). The lower right panel (d) shows the radial profiles of the time averaged $< q_i >$, $< q_e >$ and radial $E \times B$ drift intensity $< \delta v_E{}^2 >$. ITG turbulence: shows the radial profiles of the time averaged $< q_i >$, $< q_e >$ and radial $E \times B$ drift intensity $< \delta v_r{}^2 >$

The radial-time contour plots of the flux-surface averaged $< q_i >$, $< \delta\phi^2 >$, and $< q_e >$ are shown in Figs. 2(a)–2(c) respectively. The remarkable similarity between $< q_i >$ and $< \delta\phi^2 >$ in both radial structure and time evolution confirms that the ion heat transport is driven by the local fluctuation intensity. However, the electron heat flux $< q_e >$ contains a ballistic propagation in the radial direction. This indicates that the electron heat transport may contain both diffusive and pinch terms [6,7]. Therefore, the electron heat transport follows the global structure of the turbulence intensity profile but contains a nondiffusive component on the mesoscale.

TABLE I. Characteristic time scales for trapped electrons in the CTEM turbulence and for ions in the ITG turbulence.

| $[L_n/v_i]$ | $\tau_{\text{decor}}$ | $\tau_{\parallel}$ | $\tau_{\perp}$ | $\tau_{\text{eddy}}$ | $\tau_{\text{au}}$ | $\tau_s$ | $\frac{1}{\gamma_{\max}}$ |
|---|---|---|---|---|---|---|---|
| CTEM $e$ | 0.61 | $\infty$ | $\infty$ | 1.6 | 11 | 0.66 | 4.0 |
| ITG $i$ | 1.7 | 1.8 | 2.0 | 4.9 | 7.2 | 1.4 | 9.1 |

We define an effective decorrelation time $\tau_{decor}$, since both ion and electron heat transport are proportional to the turbulence intensity on the global scale, i.e., $\tau_{decor} = 4\chi_e / 3\delta v_E{}^2 \approx 0.61 L_n / v_i$, after relating the test particle diffusivity $D$ to the electron thermal conductivity $\chi_e$. This characteristic time scale may reflect the physical process relevant to the transport mechanism, which could be either kinetic wave particle decorrelation or fluid eddy mixing.

We calculate and list all the relevant characteristic time scales in Table I. Comparing to $\tau_{decor}$, the zonal flow shearing time $\tau_s$ and eddy turnover time $\tau_{eddy}$ are the two closest time scales. This suggests that the decorrelation process should be mostly the eddy mixing regulated by the zonal flows. All the kinetic time scales are much larger than $\tau_{decor}$, $\tau_s$, and $\tau_{eddy}$. Therefore, the electron heat transport in the CTEM turbulence is mainly a fluid process although the linear instability is driven by the kinetic process of the toroidal precessional resonance. The radially random distribution of the microscopic and mesoscale eddies enables the electrons to average out the local structure of the turbulence intensity.

For comparison, we perform a simulation of the ITG turbulence with adiabatic electrons with a system size of $a/\rho_i = 250$ and also list the ITG characteristic time scales in Table I. The ion heat transport is found to be a quasilinear process [8] and regulated by the wave particle decorrelation with $\tau_{\parallel} = 1/\langle \Delta k_{\parallel} v_i \rangle$ and $\tau_{\perp} = 3/\left(4\chi_i s^2 \langle \theta^2 \rangle \langle k_\theta{}^2 \rangle\right)$, using the method in Ref. [9].

The nondiffusive feature of the electron heat transport can be further confirmed by the probability distribution function (PDF) of the flux-surface-averaged electron heat flux, as shown by the circles in Fig. 3(a). If the heat transport is purely a diffusive process, the flux-surface-averaged heat flux should follow the lognormal distribution [10], which is true for the ion heat fluxes and small electron heat fluxes in Fig. 3(a). However, neither lognormal nor Gaussian distribution can fit well the simulation PDF in the whole range of the electron heat flux. There is a significant large heat flux component that is above the lognormal distribution, which indicates a nondiffusive/superdiffusive component. The large ion heat fluxes are below the lognormal distribution, which may indicate a subdiffusive component. On the contrary, the PDF of the flux-surface-averaged ion heat flux in the ITG turbulence is consistent with the lognormal distribution, as shown in Fig. 3(b), which suggests that the ion heat transport in the ITG turbulence is a diffusive process [5] .

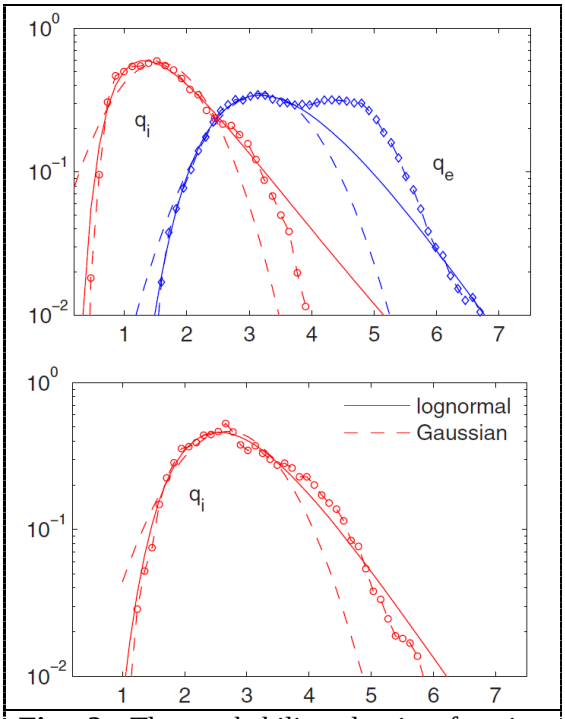


**Fig. 3**: The probability density function (PDF) of the flux-surface-averaged electron heat flux $q_e$ and ion heat flux $q_i$ in the CTEM turbulence, shown in the upper panel (a), and ion heat flux $q_i$ in the ITG turbulence, shown in the lower panel (b), with the electron heat flux normalized by $n_{tr}\nabla T_e$ and ion heat flux normalized by $n_0\nabla T_i$, where $n_{tr}$ is the trapped electron density. The solid line is a lognormal distribution fit and the dashed line is a Gaussian distribution fit.

3. Momentum transport in ITG turbulence

We carried out an ITG simulation first with adiabatic electrons to study the momentum transport [11-13]. The symmetry breaking and momentum flux generating mechanisms due to the radial electric field shearing [4] are examined. In Fig. 4(a) we compare the time-averaged profiles of the turbulence-generated zonal flow shear and the flux-surface-averaged parallel wavenumber of the turbulence, with rather strong correlation between these two profiles observed. In Fig. 4(b), we plot the radial profiles of $\langle k_\parallel \rangle \langle \delta\phi^2 \rangle$ and toroidal momentum flux. The correspondence between these profiles is characterized by the correlation coefficient C = 0.75, which also indicates strong correlation. The flux-surface-averaged parallel wavenumber $\langle k_\parallel \rangle$ is multiplied by the fluctuation intensity $\langle \delta\phi^2 \rangle$ in order to match the proper radial envelope of the momentum flux, since the profile of fluctuation intensity is smooth and then itself cannot be responsible for the strong correlation between $\langle k_\parallel \rangle \langle \delta\phi^2 \rangle$ and toroidal momentum flux. The results obtained so far confirm the role of the radial electric field shear in generating the residual stress component of the toroidal momentum flux. However, in the case of a finite background rotation (Fig. 4 (c) ), the $E\times B$ shear and momentum flux profiles show no apparent correlation (C = −0.05), suggesting that the convective flux, which is stronger than the residual stress in this case, has a different driving mechanism. Next, we carried out GTC simulation with kinetic electron and found that the trapped electrons in the ITG turbulence increase the intensity and modify the spectral properties of the electrostatic fluctuations, leading to the increase in the toroidal momentum pinch. Finally, GTC simulation of momentum transport in tokamak driven by collisionless trapped electron (CTEM) turbulence finds that diffusive momentum flux is dominant. Particle convection driven by density gradient drives outward momentum pinch competing with TEP-like inward momentum pinch. The residual stress is insignificant (~10%) There is strong correlation between ZF shearing and residual momentum flux, however it might be due to the turbulence suppression effect of ZF The direction of residual momentum flux is opposite in the ITG and CTEM turbulence

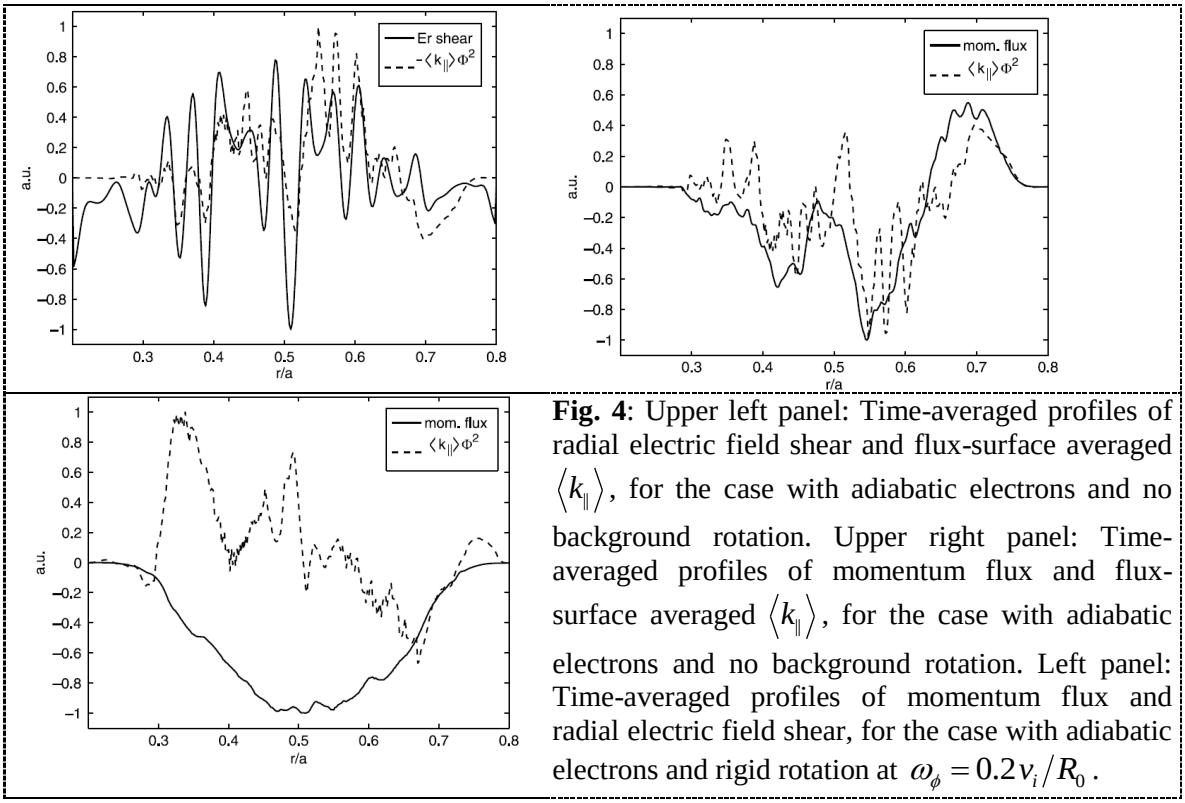


**Fig. 4**: Upper left panel: Time-averaged profiles of radial electric field shear and flux-surface averaged $\langle k_{\parallel} \rangle$, for the case with adiabatic electrons and no background rotation. Upper right panel: Time-averaged profiles of momentum flux and flux-surface averaged $\langle k_{\parallel} \rangle$, for the case with adiabatic electrons and no background rotation. Left panel: Time-averaged profiles of momentum flux and radial electric field shear, for the case with adiabatic electrons and rigid rotation at $\omega_{\phi} = 0.2 v_i / R_0$.

4. Turbulent transport in the reverse shear toroidal plasmas

Electrostatic ion temperature gradient (ITG) and trapped electron mode (TEM) turbulence in tokamak plasmas with reversed magnetic shear [3] is studied by simulations using Gyrokinetic Toroidal Code (GTC) [2]. In the ITG turbulence, electrostatic potential gaps are observed in the minimum-q region in the linear phase when $q_{min}$ is an integer. When $q_{min}$ is an integer, some rational surfaces degenerate at the minimum-q position, forming two gaps in which there is no rational surface. The potential gap has similar size as the rational surface gaps, confirming previous theories of weakening of toroidal coupling by rarefaction of rational surfaces, which generates a gap in the global mode structure. In the TEM turbulence, the mode grows only in the positive-shear side in the linear phase, because electron precessional drift velocity is decreased or reversed in the negative-shear side, breaking the precessional resonance. In the non-linear phase of both ITG and TEM turbulence, turbulence spreads into linearly stable regions. Whatever structure formed in the linear phase is destroyed. The fluctuation and transport have no significant gap across the $q_{min}$ region even when $q_{min}$ is an integer. Our finding indicates that the electrostatic drift wave turbulence itself does not support either linear or nonlinear mechanism for the formation of internal transport barriers in the reversed magnetic shear when $q_{min}$ crossing an integer.

Fig. 5(a) shows the time history of the volume averaged potential intensity $\left\langle \delta\phi^2 \right\rangle_{vol}$ excluding zonal potential. Starting from the time 96 (unit: $R_0/c_s$), nonlinear effects come into play and the ITG instability saturates. Three snapshots are taken at times 96, 112, and 128, and only the time step 96 and 128 are shown in Fig. 5 (e) and (g) to represent the typical linear and nonlinear mode structure. It is seen that the potential gap structure that forms in the linear phase is filled up after nonlinear saturation. This effect is due to turbulence spreading [14].

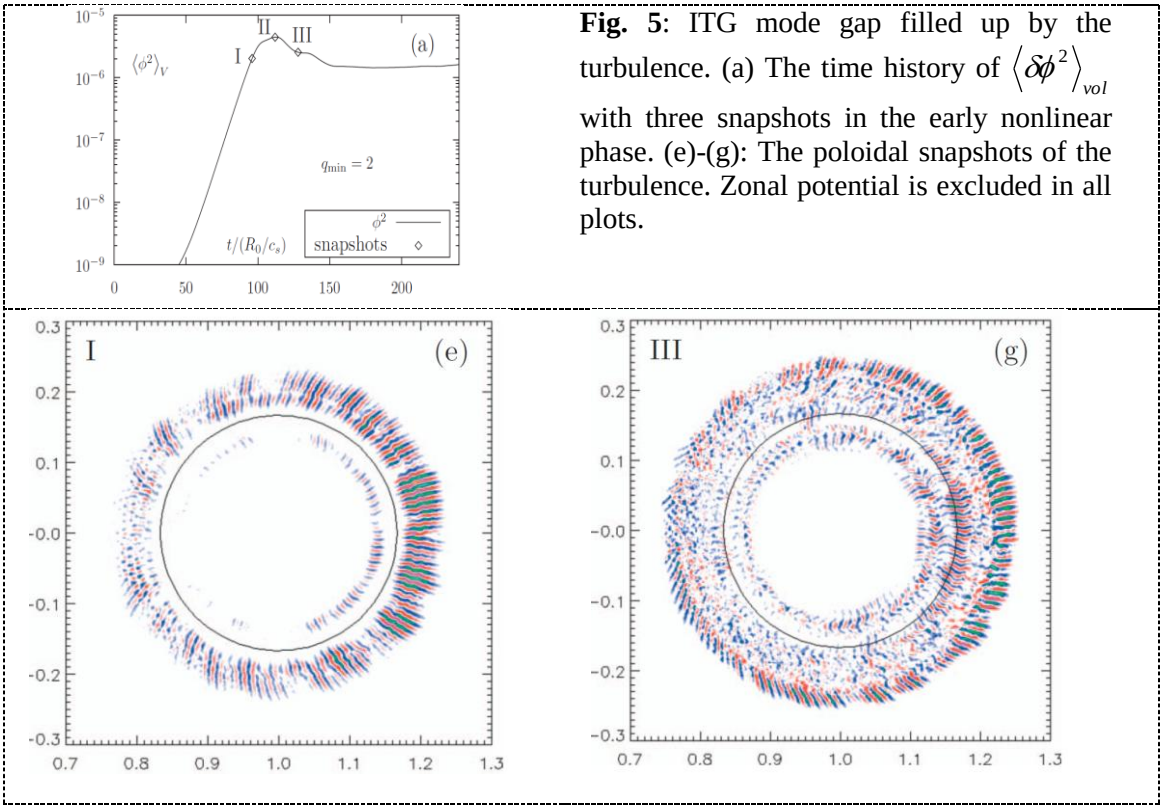


**Fig. 5**: ITG mode gap filled up by the turbulence. (a) The time history of $\left\langle \delta\phi^2 \right\rangle_{vol}$ with three snapshots in the early nonlinear phase. (e)-(g): The poloidal snapshots of the turbulence. Zonal potential is excluded in all plots.

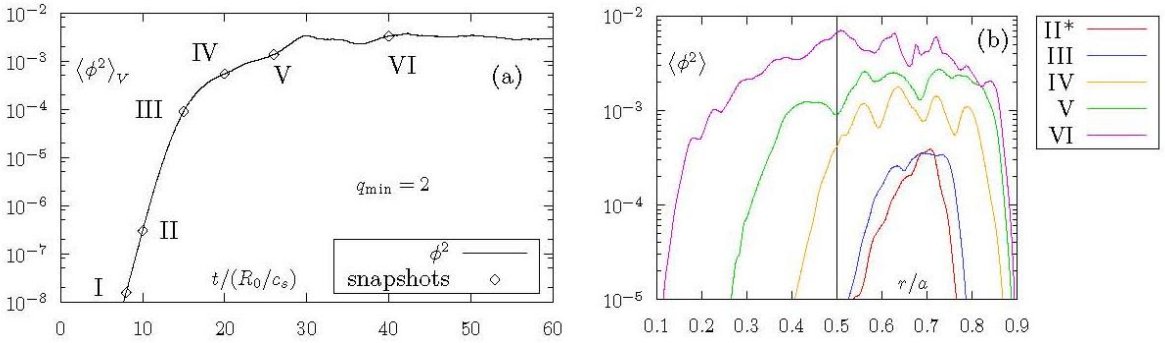


**Fig. 6**: TEM turbulence spreading from the positive-shear region into the negative-shear region (magnetic shear s < 0 for r < 0.5a and s > 0 for r > 0.5a). (a) The time history of the volume-averaged $\phi^2$. Six snapshots are taken. TEM instability saturates around snapshot IV. (b) Evolution of flux-surface-averaged $\phi^2$ in the nonlinear phase. (II*: scaled up; black line: $q_{min}$ position)

The CTEM turbulence shows similar feature like that of ITG in a reversed shear plasma [4]. In the linear phase the CTEM instability is suppressed in the negative-shear region due to the reversal of the toroidal precessional drift of trapped electrons. However, after nonlinear saturation, the CTEM fluctuation propagates into the stable negative-shear region due to the turbulence spreading as shown in Fig. 6. Our finding indicates that the electrostatic drift wave turbulence itself does not support either linear or nonlinear mechanism for the formation of internal transport barriers in the reversed magnetic shear when $q_{\min}$ crossing an integer.

Work supported by SciDAC GPS.

References:

1. Lin, Z., T. S. Hahm, W. W. Lee, W. M. Tang, and R. B. White, Science, **281**, 1835 (1998).
2. Xiao, Y. and Z.H. Lin, *Turbulent Transport of Trapped-Electron Modes in Collisionless Plasmas.* Physical Review Letters, 2009. 103(8).
3. Deng, W.J. and Z.H. Lin, *Properties of microturbulence in toroidal plasmas with reversed magnetic shear.* Physics of Plasmas, 2009. 16(10).
4. Holod, I. and Z. Lin, *Effects of electron dynamics in toroidal momentum transport driven by ion temperature gradient turbulence.* Plasma Physics and Controlled Fusion, 2010. 52(3).
5. Lin, Z., et al., *Size scaling of turbulent transport in magnetically confined plasmas.* Physical Review Letters, 2002. 88(19).
6. Basu, R., et al., *Turbulent flux and the diffusion of passive tracers in electrostatic turbulence.* Physics of Plasmas, 2003. 10(7): p. 2696-2703.
7. Vlad, M., F. Spineanu, and S. Benkadda, *Turbulent pinch in the non-homogeneous confining magnetic field.* Plasma Physics and Controlled Fusion, 2008. 50(6).
8. Holod, I. and Z. Lin, *Statistical analysis of fluctuations and noise-driven transport in particle-in-cell simulations of plasma turbulence.* Physics of Plasmas, 2007. 14(3).
9. Lin, Z., et al., *Wave-particle decorrelation and transport of anisotropic turbulence in collisionless plasmas.* Physical Review Letters, 2007. 99(26).
10. Xiao, Y., et al., *Fluctuation characteristics and transport properties of collisionless trapped electron mode turbulence.* Physics of Plasmas, 2010. 17(2).
11. Peeters, A.G., C. Angioni, and D. Strintzi, *Toroidal momentum pinch velocity due to the coriolis drift effect on small scale instabilities in a toroidal plasma.* Physical Review Letters, 2007. 98(26).
12. Hahm, T.S., et al., *Turbulent equipartition theory of toroidal momentum pinch.* Physics of Plasmas, 2008. 15(5).
13. Diamond, P.H., et al., *Physics of non-diffusive turbulent transport of momentum and the origins of spontaneous rotation in tokamaks.* Nuclear Fusion, 2009. 49(4).
14. Lin, Z. and T.S. Hahm, *Turbulence spreading and transport scaling in global gyrokinetic particle simulations.* Physics of Plasmas, 2004. 11(3): p. 1099-1108.